Geomorphology 123 (2010) 279–289

Contents lists available at ScienceDirect

Geomorphology

journal homepage: www.elsevier.com/locate/geomorph

Potential impacts of agricultural expansion and climate change on soil erosion in the Eastern Arc Mountains of Kenya

Eduardo Eiji Maeda *, Petri K.E. Pellikka, Mika Siljander, Barnaby J.F. Clark

University of Helsinki, Department of Geosciences and Geography, Gustaf Hällströmin katu 2, 00014, Helsinki, Finland

ARTICLE INFO

Article history:
Received 3 April 2010
Received in revised form 21 July 2010
Accepted 23 July 2010
Available online 1 August 2010

Keywords:
Agricultural expansion
Soil erosion
Simulation models
Climate change
Taita Hills

ABSTRACT

The Taita Hills form the northernmost part of the Eastern Arc Mountains of Kenya and Tanzania, is one of the world's most important regions for biological conservation. Due to the expansion of agricultural activities during the last centuries, currently only 1% of the original vegetation remains preserved in the Taita Hills. These landscape changes, together with potential increases in rainfall volumes caused by climate change, offer a great risk for soil conservation. The present research aims to evaluate how future changes in climate and land use can alter, in time and space, the variables inherent to a widely used soil erosion model, and to assess the impacts of these changes for soil conservation. A modelling framework was assembled by integrating a landscape dynamic model, a soil erosion model and synthetic precipitation datasets generated through a Monte Carlo simulation. The results indicate that, if the current trends persist, agricultural areas will occupy roughly 60% of the study area by 2030. Although these land use changes will certainly increase soil erosion figures, new croplands will likely take place predominantly in the lowlands, which comprises areas with lower soil erosion potential. By the year 2030, rainfall erosivity is likely to increase during April and November, while a slight decrease tendency is observed during March and May. An integrated assessment of these environmental changes, performed using the modelling framework, allows a clear distinction of priority regions for soil conservation policies during the next 20 years.

1. Introduction

The replacement of forests, wetlands, savannahs and other native landscapes is a severe threat in the capacity of the environment to sustain food production, maintain freshwater and other ecosystem services (Foley et al., 2005). Currently, almost one-third of the world's land surface is under agricultural use and millions of hectares of natural ecosystems are converted to croplands or pastures every year. In sub-Saharan Africa, 16% of the forests and 5% of the open woodlands and bushlands were lost between 1975 and 2000, while the agricultural land has expanded 55% and agricultural production has increased almost 50% (Brink and Eva, 2009).

Anthropogenic changes in the environment are also affecting the global climate (IPCC, 2007). Changes in precipitation and temperature patterns will likely have important impacts on the sustainability of agricultural systems. For instance, it is expected that without proper investments in water management, climate changes may increase in roughly 20% the global irrigation water needs by 2080 (Fischer et al., 2007). Climate changes may also adversely affect agricultural production, access to food and stability of food supplies, having direct impacts on food security (Schmidhuber and Tubiello, 2007).

The association of climate changes and land cover changes is particularly threatening soil conservation. The natural vegetation protects the soil against the impacts of rainfall and it is a source of organic matter to the soil. These factors improve infiltration and enhance the recharging of groundwater reservoirs. When vegetation cover is displaced, infiltration capacity is decreased, resulting in surface runoff, which will carry sediments and nutrients into rivers (Van Oost et al., 2000; Zuazo and Pleguezuelo, 2008). Moreover, changes in precipitation volume and intensity caused by climate changes may increase the energy available in rainfall for detaching and carrying sediments. According to Yang et al. (2003), the global average soil erosion is projected to increase approximately 9% by 2090 due to climate changes.

Although soil erosion is a natural and inevitable process, the accelerated rates of soil loss, caused by the factors mentioned above, represent a serious environmental problem. For instance, increased rates of soil erosion are directly associated with nutrient loss, which may reduce agricultural productivity (Bakker et al., 2007) and cause water bodies' eutrophication (Istvánovics, 2009). In some cases, advanced stages of soil erosion, such as rill and gully erosions, can devastate entire areas, turning them unusable for agricultural purposes (Valentin et al., 2005; Kirkby and Bracken, 2009).

In this context, the improvement of models and computer capacity in the past decades allowed an increasing number of studies aiming at the sustainable use of natural resources and land use planning. For

* Corresponding author. Tel.: +358 44 2082876.
E-mail address: eduardo.maeda@helsinki.fi (E.E. Maeda).

0169-555X/$ – see front matter © 2010 Elsevier B.V. All rights reserved.
doi:10.1016/j.geomorph.2010.07.019

instance, land use and land cover change (LUCC) simulation models provide robust frameworks to cope with the complexity of land use systems (Veldkamp and Lambin, 2001). Such models are considered efficient tools to project alternative scenarios into the future and to test the stability of interrelated ecological systems (Koomen et al., 2008). Soil erosion models, in turn, are designed to estimate soil loss figures by simulating the processes involved in the detachment, transport and deposition of sediments. Existing soil erosion models vary in terms of complexity and data requirement. The concept of such models can be based on empirical observations, physical equations or a combination of both (Merritt et al., 2003).

Nevertheless, land use and soil erosion are closely linked with each other, with local climate and with society, assembling a very complex system. Although many studies have been undertaken to separately understand each of these processes, scientists currently face the challenge to integrate these studies into more complex frameworks. The understanding of these interconnected relations is an essential step for elaborating public policies that can effectively lead to the conservation of natural resources.

In this study, an integrated modelling framework was assembled in order to investigate the potential impacts of agricultural expansion and climate changes on soil erosion in the Taita Hills, Kenya. The Taita Hills are home for an outstanding diversity of flora and fauna and a high level of endemism (Burgess et al., 2007). The landscape of the Taita Hills has been drastically changed during the past centuries due to agricultural expansion, and soil erosion problems have been identified in the area (Sirviö et al., 2004). Hence, the region is considered to have exceptional importance for biological and natural resources conservation.

2. Study area

The Taita Hills are located in the northernmost part of the Eastern Arc Mountains of Kenya and Tanzania, in the middle of the Tsavo plains of the Coast Province, Kenya (Fig. 1). The Taita Hills cover an area of approximately 850 km^2. The population of the whole Taita-Taveta district has grown from 90,146 in 1962 persons to over 300,000 in 1999 (Republic of Kenya, 2001). The indigenous cloud forests have suffered substantial loss and degradation for several centuries as they have been converted to agriculture, because of the abundant rainfall and rich soils that provide good conditions for agricultural production (Clark and Pellikka, 2009). Approximately half of the cloud forests in the hills has been cleared for agricultural lands since 1955 (Pellikka et al., 2009), but on the other hand the forest cover is not drastically changed due to introduction of exotic plantations. Currently, only 1% of the original forested area remains preserved.

Located in the inter-tropical convergence zone, the area has a bimodal rainfall pattern, the long rains occurring in March–May and short rains in November December. The agriculture in the hills is intensive small-scale subsistence farming. In the lower highland zone and in upper midland zone, the typical crops are maize, beans, peas, potatoes, cabbages, tomatoes, cassava and banana. In the slopes and lower parts of the hills with average annual rainfall between 600 and 900 mm, early maturing maize species and sorghum and millet species are cultivated. In the lower midland zones with average rainfall between 500 and 700 mm, dryland maize types and onions are cultivated. The two growing seasons, totaling to 150 170 days, coincide with the long and the short rains (Jaetzold and Schmidt, 1983). The land is prepared during the dry season, and the crops are seeded prior to the short rains and long rains. Harvesting takes place after the end of the rainy seasons.

3. Material and methods

In the presented research future agricultural expansion and climate change scenarios were simulated in order to evaluate their potential impacts on soil erosion in the Taita Hills, Kenya. To achieve this objective a modelling framework was assembled by coupling a landscape dynamic simulation model, an erosion model and synthetic precipitation datasets generated through a Monte Carlo simulation. The purpose of this framework was to evaluate how future changes in climate and land cover can alter, in time and space, the variables inherent to a widely used soil erosion model.

Remote sensing and GIS techniques were combined to provide the necessary inputs for the modelling framework. A flow chart illustrating the components of the modelling framework is presented in Fig. 2, and the main components involved in the study are described in detail below.

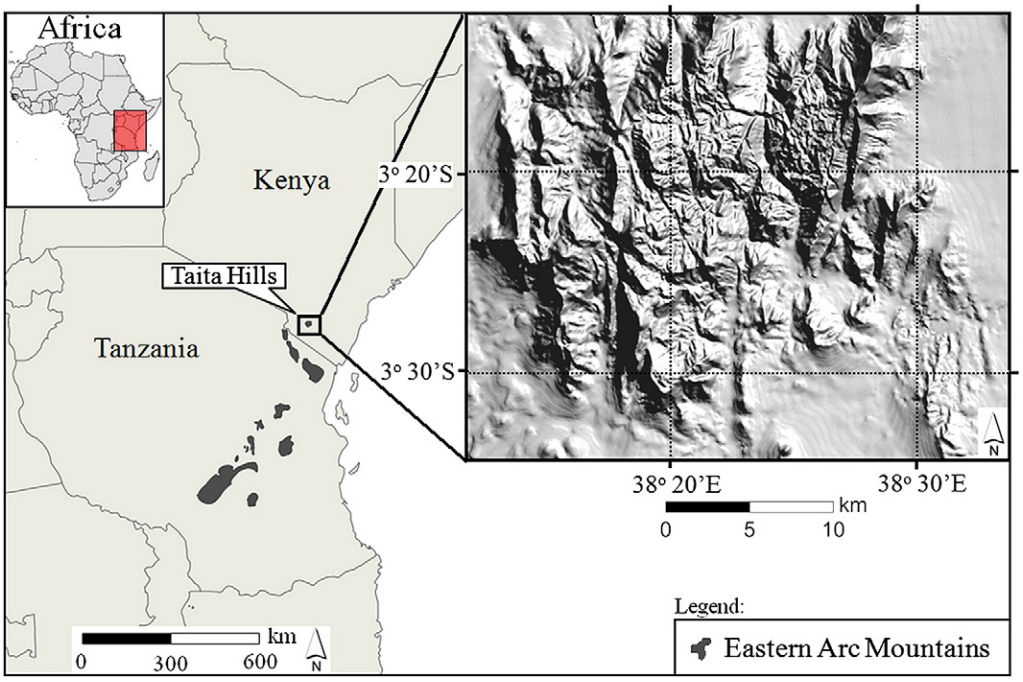

Fig. 1. Geographic location of the Taita Hills. The detail shows the Digital Elevation Model shaded-relief of the study area.

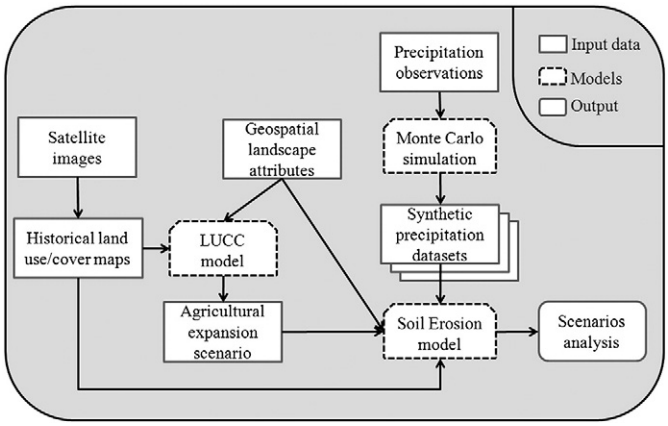

Fig. 2. Flow chart illustrating the integrated modelling framework concept.

3.1. Agricultural expansion model

Dynamic models operating on a cellular automata basis have arisen as a feasible alternative for the analysis of land use dynamics and in the exploration of future landscape scenarios. In this study, a spatially explicit simulation model of landscape dynamics, DINAMICA-EGO (Soares-Filho et al., 2002, 2009), was applied to simulate future scenarios of land use in the Taita Hills. The model receives as inputs land use transition rates, landscape variables and landscape parameters. The landscape parameters are intrinsic spatially distributed features, such as soil type and slope, which are kept constant during the simulation process. The landscape variables are spatio-temporal dynamic features that are subjected to changes by decision makers, for instance roads and protected areas.

The model was driven by land use and land cover maps (LULCM) from two selected dates (Clark and Pellikka, 2009): 1987 (initial landscape) and 2003 (final landscape), which are used as inputs to represent the historical land use transitions in the study area. The dates of the LULCM were chosen based on two criteria. The first criterion was that the landscape changes between the initial and final landscape should accurately represent the ongoing land change activities in the study area. That is to say, the agricultural expansion rates between 1987 and 2003 were assumed to retrieve a consistent figure of the current trends. The second criterion relied on the availability of cloud free satellite images to assemble the LULCM. In total, ten landscape attributes (variables/parameters) were used as inputs for the model: distance to roads, distance to markets, altitude, distance to rivers, protected areas, soil type, slope, insolation, mean annual precipitation and distance to already established croplands. All landscape attributes were represented by raster images with a 20 m spatial resolution.

After the transition rates are defined and the role of each landscape attributed is evaluated, the model uses stochastic algorithms to allocate land changes and simulate landscape scenarios (Almeida et al., 2005). In this study, the LULCM from the year 2003 was considered to be the initial landscape and the model was applied to simulate land changes up to 2030. In this case, an exploratory scenario was simulated. An exploratory scenario is a sequence of emerging events (Alcamo, 2001). Namely, the average agricultural expansion rates observed from 1987 to 2003 in the study area were used to build an exploratory scenario with stationary behaviour for the year 2030.

The model performance for the study area was evaluated in a previous study (Maeda et al., 2010) using a method proposed by Hagen (2003), in which multiple resolution windows are used to compare the simulated and the reference maps within a neighbourhood context. The performance achieved in the LUCC model calibration was considered satisfactory, achieving spatial fittings from 75%, at a spatial resolution of 100 m, up to 90% at a spatial resolution of 380 m.

3.2. Synthetic precipitation datasets

Climate change scenarios simulated by General Circulation Models (GCMs) generally provide datasets at spatial resolutions that are considered too coarse for studies at local scales. Moreover, many spatial downscaling approaches, such as dynamic downscaling, require additional datasets that are frequently unavailable in poor countries. Hence, a simplified approach was carried out to generate synthetic precipitation datasets and simulate plausible climate change scenarios for the study area.

Firstly, high spatial resolution precipitation grids were created by interpolating rainfall observations from the Kenya Meteorological Department obtained from eleven ground stations in the Taita Hills and surrounding lowlands. The interpolation was carried out using the ANUSPLINE software (Hutchinson, 1995). In total, 17 years of observations, from 1989 to 2005, were used to create monthly average rainfall maps. Next, the probability distribution function (PDF) for monthly precipitation was estimated in each point of the grid using a gamma distribution function. The gamma distribution was chosen for being able to provide flexible representation of a variety of distribution shapes (Wilks, 1990). Moreover, this type of distribution has been successfully applied in recent studies to represent monthly rainfall in East Africa (Husak et al., 2007). The gamma PDF $f(x)$ is given by:

$$f(x|a,b) = \frac{1}{b^a \Gamma(a)} x^{a-1} e^{\frac{x}{b}} \quad (1)$$

$$\Gamma(a) = \int_0^\infty e^{-t} t^{a-1} dt \quad (2)$$

where a and b are the distribution parameters and Γ is the gamma function. The parameters of the distribution were estimated in the software MATLAB™ using the maximum likelihood approach. After the parameters were solved for every point in the grid, a Monte Carlo simulation was carried out to generate synthetic monthly precipitation datasets. For the simulation, 100 random values were extracted from the PDF in each point of the grid, to represent an estimated monthly volume of precipitation. The synthetic precipitation observation in the point is then considered to be the average of the 100 iterations.

Four synthetic precipitation datasets were generated for this study in order to simulate different scenarios. In the first scenario (Sy), a synthetic precipitation dataset was generated by running the Monte Carlo simulation using the same characteristics observed in the historical dataset (1989 to 2005). In other words, the Sy represents the monthly precipitations in a scenario without climate change. Throughout the present study the Sy scenario is considered the reference for comparisons with the climate change scenarios.

In the three other scenarios, climatic changes were simulated by perturbing the PDF during the Monte Carlo simulation. In order to delineate plausible scenarios, the PDFs were perturbed based on precipitation responses to climate change (percent changes) simulated by a GCM between the years 2011 2030. Given the coarser spatial resolution of the GCM, just the GCM grid point closest to the study area was used as reference for the precipitation response values.

The GCM chosen to be used in the presented study was the ECHAM version 5, developed at the Max Planck Institute for Meteorology in Hamburg. In a comparison with five other GCMs the ECHAM achieved the best results in simulating the rainfall patterns in the East-African region (McHugh, 2005). Moreover, the ECHAM was successfully used in recent studies aiming to evaluate the impacts of climate changes on agricultural systems in East Africa (Thornton et al., 2009, 2010).

The climate changes simulated by the ECHAM5 for three greenhouse-gas emission scenarios (SRES, Special Report on Emissions Scenarios) were used as reference in this study for perturbing the precipitation PDFs. Namely, the emission scenarios SRA1B, SRA2 and SRB1

(Nakicenovic et al., 2000) were used to generate three synthetic precipitation datasets: SyA1B, SyA2 and SyB1, respectively. The data necessary for this procedure were obtained from the IPCC data distribution centre (http://www.ipcc-data.org).

The SRA1B emission scenario simulates a future world of rapid economic growth, low population growth and rapid introduction of new and more efficient technology. The SRA2 scenario represents a very heterogeneous world, with high population growth, slower technological changes and less concern for rapid economic development. Lastly, the SRB1 simulates a world with rapid changes in economic structures toward a service and information economy, with the introduction of clean and resource-efficient technologies (IPCC, 2007).

3.3. Soil erosion model

The LUCC model and the synthetic precipitation datasets were integrated with a soil erosion model. The objective of this approach was to evaluate how agricultural expansion, together with climate change, can modify the variables of a widely used soil erosion model, allowing a quantitative and qualitative assessment of the impacts of these changes for soil conservation. The soil erosion model used in this study was the Universal Soil Loss Equation (USLE) (Wischmeier and Smith, 1978).

The USLE and its revised version, RUSLE (Renard et al., 1997), have been extensively used worldwide during the last decades (Kinnell, 2010). Even though these models are known for their simplicity, their effectiveness has been demonstrated in many recent studies (e.g. Beskow et al., 2009; Terranova et al., 2009; Nigel and Rughooputh, 2010). The USLE is given as:

$$A = R \times K \times LS \times C \times P \tag{3}$$

where A is the annual average soil loss [t ha^{-1} year^{-1}], R is the rainfall erosivity factor [MJ mm ha^{-1} h^{-1}], K is soil erodibility [t ha h MJ^{-1} mm^{-1}], LS is the topographical factor [-], C is the vegetation cover factor [-], and P represents erosion control practices [-].

Provided the fact that the K and LS factors are intrinsic characteristics of the landscape, they can be kept constant in all simulated scenarios. On the other hand, LUCC directly affect the C factor. The changes were analysed by evaluating the average C factor value in the study area during 1987, 2003 and in the simulated scenario for 2030. The potential impacts of agricultural expansion for soil conservation were also assessed by analysing the spatial distribution of croplands in relation to the K and LS factors. Possible changes in the P factor were not addressed in the present study.

The rainfall erosivity factor (R) is a numerical index that expresses the capacity of the rain to erode a soil (Wischmeier and Smith, 1978). Hence, the R factor is directly affected by changes in precipitation pattern. These changes were evaluated at monthly and yearly time steps. Additionally, the soil erosion potential was calculated by excluding the anthropogenic variables from the USLE equation (C and P). This approach is needed to clearly understand the role of external factors in the system, without the influence of the changes in the landscape cause by human activities.

Although the USLE provides a simple and useful tool for soil conservation, studies commonly neglect the calibration and validation of this model. Given the absence of reliable data for calibration, the presented study did not attempt to provide soil loss estimation figures. Instead, the evaluation of the soil erosion potential among the different scenarios was based mainly on a comparative analysis of changes, following the procedure proposed by Miller et al. (2002) and Kepner et al. (2004). Such procedure assumes that, using percent change observations, the parameters incorporated in an eventual calibration would be partially or totally cancelled, providing more realistic figures than absolute values of soil loss. We analyzed the absolute changes in soil erosion potential only qualitatively, taking into account the spatio-temporal distribution of changes.

The R factor was calculated using the method proposed by Renard and Freimund (1994), and recently applied in Beskow et al. (2009). The method is based on an empirical relationship between rainfall erosivity and the Fournier Index (FI; Fournier, 1960). FI gives indication of climatic aggressiveness, which has a high correlation with the amount of sediment washed into the stream by surface runoff. The R factor was calculated as follows:

$$FI = \frac{p_i^2}{p} \tag{4}$$

$$r_i = \frac{125.92 \times FI^{0.603} + 111.173 \times FI^{0.691} + 68.73 \times FI^{0.841}}{3} \tag{5}$$

$$R = \sum_{i=1}^{12} r_i \tag{6}$$

where p_i is the average monthly rainfall [mm] for month i, P is the mean annual precipitation [mm], and r_i is the average monthly erosivity [MJ mm ha^{-1} h^{-1} month^{-1}].

The K factor was calculated using the method proposed by Williams and Renard (1983). This approach was chosen for being broadly used in recent studies (e.g. Xiaodan et al., 2004; Rahman et al., 2009) and for requiring input variables that are commonly available worldwide. The method is described by the following equations:

$$K = \left\{0.2 + 0.3\exp\left[-0.0256\,Sd\left(1-\frac{Si}{100}\right)\right]\right\} \times \left[\frac{Si}{(Cl+Si)}\right]^{0.3} \times \{1-0.25C/[C+\exp(3.72-2.95C)]\} \times \left\{\frac{(1-0.7SN)}{[SN+\exp(5.51+22.9SN)]}\right\} \tag{7}$$

$$SN = \frac{1-Sd}{100} \tag{8}$$

where Sd is the content of sand (%), Si is the content of silt (%), Cl is the content of clay (%), and C is the content of organic carbon (%). Subsequently, the K factor units were properly converted to the SI. The data necessary for these calculations were obtained from the Soil and Terrain Database for Kenya (KENSOTER), which provides a harmonized set of soil parameter estimates for Kenya (Batjes and Gicheru, 2004). The KENSOTER dataset was compiled by the Kenya Soil Survey and the World Soil Information (ISRIC), according to the SOTER (Soil Terrain Database) methodology. The SOTER approach allows the characterization of areas with individual patterns of landform, surface form, slope, parent material, and soils (Batjes et al., 2007). The KENSOTER dataset version 2.0 is available at a scale of 1:1,000,000.

The LS factor was calculated in the software USLE2D (Van Oost et al., 2000), using the algorithm proposed by Wischmeier and Smith (1978). This calculation was performed based on a 20 m spatial resolution Digital Elevation Model (DEM) interpolated from 50-foot interval contours captured from 1:50,000 scale topographic maps (Clark, 2010). The estimated altimetric accuracy of the DEM was ± 8 m and the planimetric accuracy of ± 50 m.

4. Results

The land cover maps resulted from the classification of the SPOT images and the landscape scenario for the year 2030, simulated using the LUCC model, are shown in Fig. 3. The overall accuracy of the 2003 land cover map was 89%, with a Kappa index for agreement of 0.87 (Clark and Pellikka, 2009). Accuracies were good with the croplands class, for example, having a producer's accuracy of 96% and a user's

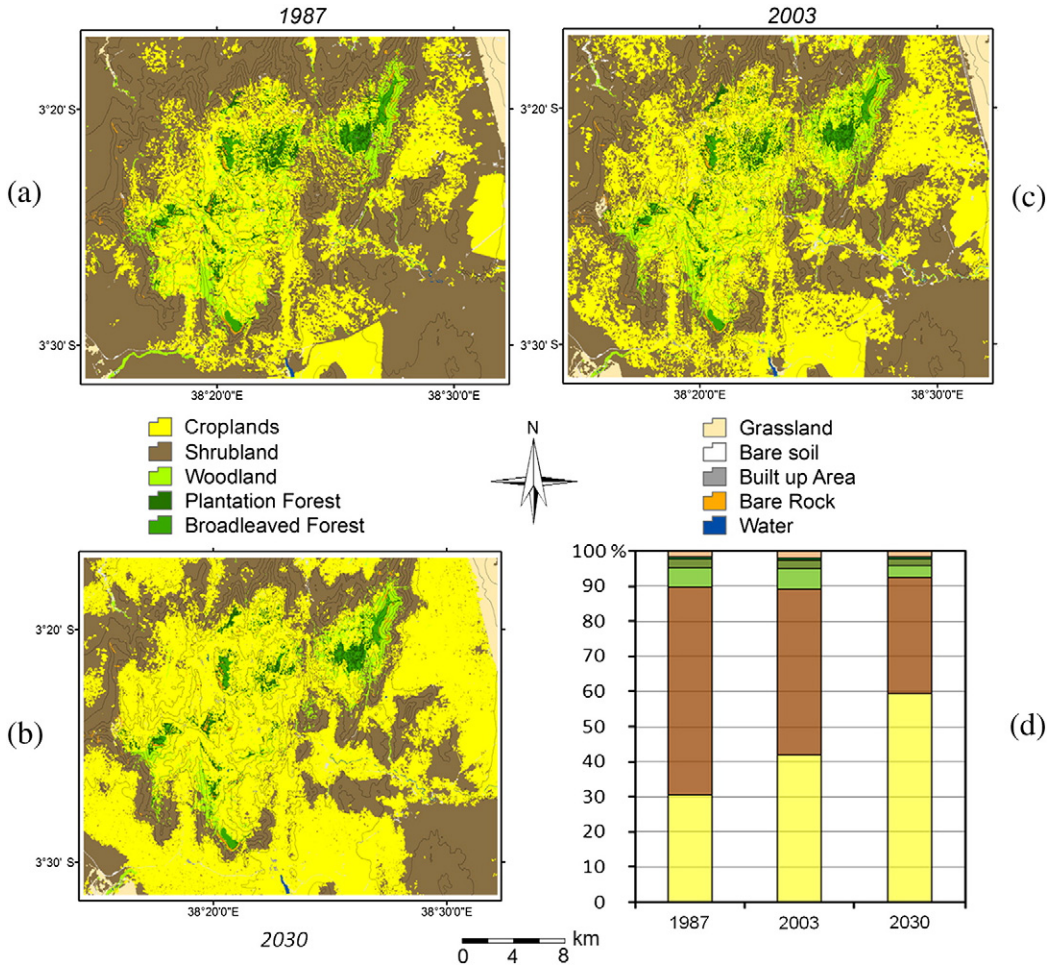

Fig. 3. Historical and simulated land use/cover changes between 1987 and 2030. (a) Historical land cover map for 1987; (b) that for 2003; (c) simulated exploratory scenario for 2030; and (d) percentage of the land cover classes in studied years.

accuracy of 82%. The exception was the lower producer accuracies of the shrubland and grassland classes, due to misclassification errors with certain areas of cropland where either shrub-like or grass-like crops gave very similar spectral and textural characteristics in the SPOT imagery. Because of a lack of timely ground reference test data or aerial photography, the accuracy of the 1987 classification could not be assessed directly. However, given the same classification methodology was applied to both scenes, the 1987 map accuracy was assumed to be similar to that of the 2003 map.

The annual average agricultural expansion rates observed from 1987 to 2003 are shown in Table 1. The highest conversion rates were observed in the transition from woodlands to agriculture. However, according to absolute numbers, shrubland areas are the most affected, given that currently they represent the predominant vegetation type in the region. The small regions covered with broadleaved forests were nearly untouched, presenting low conversion rates, and the total area decreased from 7.7 to 6.9 km^2 during the observed period.

Table 1
Annual average agricultural expansion rates.

Original vegetation	Annual conversion rate (%) (baseline 1987 2003)
Shrubland	1.305
Woodland	2.013
Plantation forest	1.161
Broadleaved forest	0.289
Grassland	0.310

In 1987 croplands were already clearly established in the Taita Hills (central area in the maps). This is explained by the favourable climatic and edaphic conditions for agricultural activities (e.g. high precipitation rates), which resulted in the clearance of large areas of forest during the last century. Between 1987 and 2003, croplands started to be implemented with higher intensity on the lowlands, provided that suitable areas for agriculture activities in the hills had already been taken almost entirely. This trend is clearly reflected in the LUCC simulation results. In the simulated scenario, the cropland areas expanded to around 515 km^2 in 2030, corresponding to about 60% of the study area. This represents an increase of 40% in comparison to the year 2003, when croplands occupied around 365 km^2.

These land changes have direct impact on the vegetation cover factor of the USLE model. Previous studies have shown that croplands increase soil exposure to weathering more than original vegetation such as forests or shrublands. For this reason the *C* factor of agricultural areas are usually higher, resulting in increased soil erosion rates. The *C* factor values used for this same area by Erdogan et al. in press indicate that average *C* increased from 0.165 in the year 1987 to 0.181 in 2003, representing an increase of 9.6%. In the LUCC simulation for the year 2030, *C* increased by 8.8% from 2003, reaching 0.197.

The distribution of cropland patches, for each of the analysed years in relation to the *LS* factor is presented in Fig. 4. As easily deduced from Eq. (3), areas with higher *LS* values are likely to undergo higher

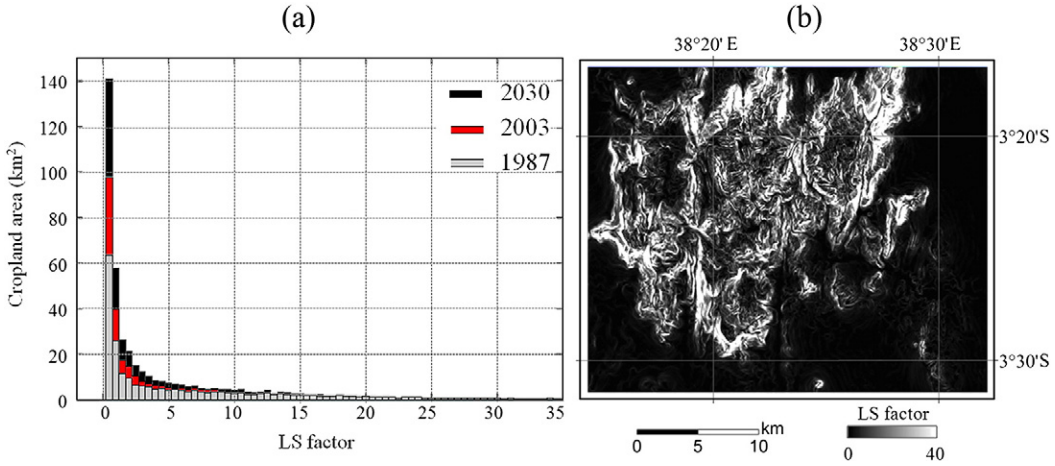

Fig. 4. Distribution of cropland patches in relation to the USLE *LS* factor. (a) Histogram showing the distribution of cropland patches in relation to the *LS* factor during the years 1987, 2003 and simulated 2030. (b) *LS* factor for the entire study area.

soil erosion rates. In the year 1987 it is observed that croplands were predominantly concentrated in areas with low *LS* values (between 0 and 10), with the highest number of patches having *LS* between 0 and 1. Between 1987 and 2003 new croplands also developed in areas with low *LS*. In other words, agricultural patches established in the last decades were mainly settled in areas with favourable topography. This pattern was reinforced after 1987, when the availability of space in the hills was scarce and the agriculture started expanding to flat areas along the foothills. In the agricultural expansion simulated for 2030, a slight increase in cropland patches has occurred in areas with *LS* between 1 and 10; however, the most significant increase has occurred again in areas with *LS* between 0 and 1 (Fig. 4a).

The soil erodibility factor in the study area varied from 0.0139 to 0.0307, allowing the distinction of eight different classes, arbitrarily named here with letters A to H (Table 2). Because soil erodibility figures may vary according to the method used for calculations, the results were analysed only in a comparative way. The spatio-temporal distribution of croplands in relation to the soil erodibility is shown in Fig. 5. In 1987 and 2003 agricultural areas were established mainly in soils with medium erodibility, namely soils B, C and D. The simulated agricultural expansion for 2030 was also higher in these soils. The low occurrence of agricultural activities in soils with high erosivity (G and H) is explained firstly by the small area occupied by these soils and secondly by the fact that such soils, together with climatic variables, create unfavourable conditions for agricultural practices. Therefore, the results indicate that agricultural activities are unlikely to expand into areas with higher soil erodibility.

Table 2
Granulometry, soil erodibility factor and classes attributed for each soil found in the study area.

ID	*Sd* (%)	*Si* (%)	*Cl* (%)	*C* (%)	*K* factor	Class
KE289	61	2	37	0.63	0.0139	A
KE251	74	8	18	0.70	0.0205	B
KE244	30	10	60	1.60	0.0205	
KE248	58	10	32	0.80	0.0228	C
KE288	50	13	37	0.69	0.0255	D
KE83	61	26	13	6.45	0.0255	
KE82	54	26	20	5.90	0.0255	
KE79	63	16	21	0.66	0.0273	E
KE56	60	19	21	0.87	0.0283	F
KE226	50	20	30	1.00	0.0283	
KE231	20	30	50	3.00	0.0302	G
KE165	50	20	30	0.20	0.0307	H

Where: *ID* = soil identification number attributed in the Soil and Terrain Database for Kenya (KENSOTER); *Sd* = content of sand (%); *Si* = content of silt (%); *Cl* = content of clay (%); *C* = content of organic carbon (%); Class = soil class arbitrarily attributed considering the USLE *K* factor.

The monthly rainfall erosivity averages for the study area, estimated using the synthetic rainfall datasets, are shown in Fig. 6. The erosivity values obtained in the SyA2 scenario resulted in the most evident differences in comparison with the Sy scenario. In January, March, May and December the changes in precipitation resulted in a clear, but slight, decrease in rainfall erosivity. The erosivity reduction during these months varied from 4 to 120 MJ mm ha^{-1} h^{-1} $month^{-1}$. On the other hand, still for the SyA2 scenario, a large increase was observed in April (280 MJ mm ha^{-1} h^{-1} $month^{-1}$) and November (260 MJ mm ha^{-1} h^{-1} $month^{-1}$).

For the SyB1 scenario, the increases in rainfall erosivity during April and November were lower, approximately 217 and 40 MJ mm ha^{-1} h^{-1} $month^{-1}$, respectively. A slight decrease was also observed during March, May and December, but in contrast with the SyA2 scenario, the erosivity during January was kept almost constant, with a minor increase of 27 MJ mm ha^{-1} h^{-1} $month^{-1}$. The SyA1B was the most conservative scenario, although clear changes are still present. It showed the highest erosivity increases during January and December, while it confirmed the tendency of a decrease in erosivity during March and May.

In general, it is plausible to assert that the climate changes simulated for the study area will likely decrease rainfall erosivity during March and May, due to a slight reduction in precipitation rates in these months. However, the model indicates the possibility of an increase, of much higher magnitudes, during April and November. The disagreements between the simulated scenarios in January and December indicate large uncertainties during these months. For June, July, August and September rainfall erosivity values are likely to continue to be very low.

The USLE *R* factors calculated for the study area are displayed in Fig. 7. Fig. 7e,f illustrates the spatial profiles of the rainfall erosivity along two transects (A′–B′ and C′–D′). For all simulated scenarios it is noted that low or no change occurs in the lowlands (roughly 500 m above sea level). The changes, however, start to be more evident along areas higher than 1000 m a.s.l., where precipitation rates are historically higher. In particular for the SyA2 scenario, changes are very high above 1500 m a.s.l., reaching absolute differences up to 1500 MJ mm ha^{-1} h^{-1} $year^{-1}$ when compared with the Sy scenario. The SyB1 scenario follows the same profile in a lower magnitude, however, resulting in erosivity increases up to 600 MJ mm ha^{-1} h^{-1} $year^{-1}$. In contrast, the SyA1B scenario did not result in marked erosivity increases and in some areas of the southwestern study area slight decreases were observed up to 60 MJ mm ha^{-1} h^{-1} $year^{-1}$. The highest increases in this scenario reached approximately 200 MJ mm ha^{-1} h^{-1} $year^{-1}$ in the hills in the northeastern study area.

Fig. 8 shows the differences observed in the soil erosion potential calculated for the climate change scenarios (SyA1B, SyA1 and SyB1)

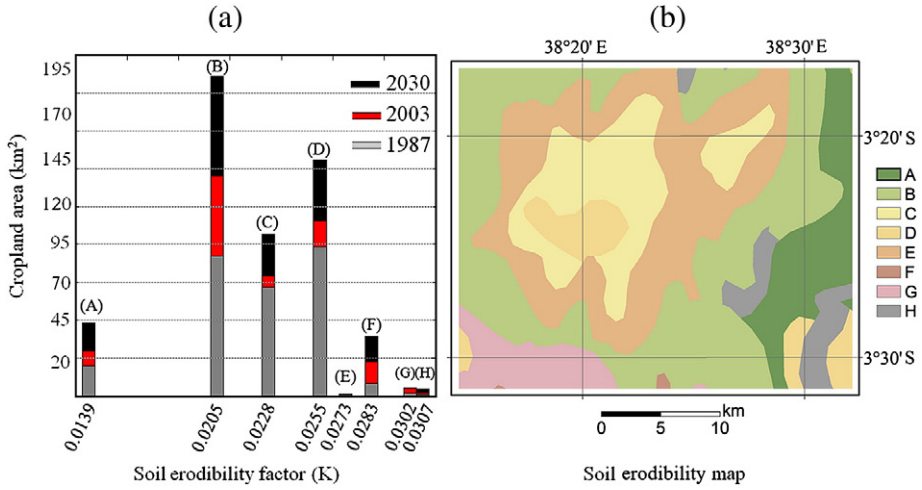

Fig. 5. Spatio-temporal distribution of croplands in relation to the soil erodibility. (a) Histogram showing the distribution of cropland patches in relation to the soil erodibility during the years 1987, 2003 and simulated 2030. (b) Spatial distribution of the soil erodibility factor in the study area.

and the scenario simulating the same characteristics as in the historical datasets (Sy). The maps at the top part of the figure show the absolute differences. In this case, given that the erosion model is not calibrated, just a qualitative analysis is performed. A numerical assessment is carried out for the maps located at the bottom part of the figure, which show the percentage changes in the soil erosion potential.

It is interesting to note that completely different patterns are observed in the absolute and percentage changes. The percentage changes correspond strongly to altitude, because in lowlands, where precipitation volumes are lower, even small changes in precipitation can lead to high percentage differences in rainfall erosivity. However, in absolute values such differences are much smaller when compared with erosivity variation in the highland with much higher precipitation rates. The percentage changes ranged from −3 to 14%. The negative values were observed only for the SyA1B scenario, evidently in the same regions where the rainfall erosivity was reduced. The patterns observed in the absolute changes are closely driven by the *LS* factor. This characteristic is driven by the fact that the *LS* factor range of values within the study area is relatively wide, and small changes in the *R* factor are more easily noticed in regions with higher *LS* values.

5. Discussion

Although early agricultural activities in the Taita Hills were initially settled in areas with higher precipitation rates (Pellikka et al., 2009), the results demonstrate that croplands were arranged by producers in areas with lower erosion risk. Namely, croplands were historically placed in areas with moderate slopes and favourable soils. It could then be feasible to expect that agricultural expansion pressure would drive rural activities to areas with higher erosion risk. However, such hypothesis is refuted based on the presented results. As shown in the LUCC simulation, croplands are likely expanding to the lowlands, where the topography is comparatively smooth and precipitation rates were historically low. Nevertheless, agricultural expansion will inevitably result in increased soil erosion due to changes in vegetation cover, as it is evidenced by increases in the USLE *C* factor. Such effect of LUCC on soil erosion has been demonstrated in numerous studies (e.g. Maeda et al., 2008; Schiettecatte et al., 2008; García-Ruiz, 2010).

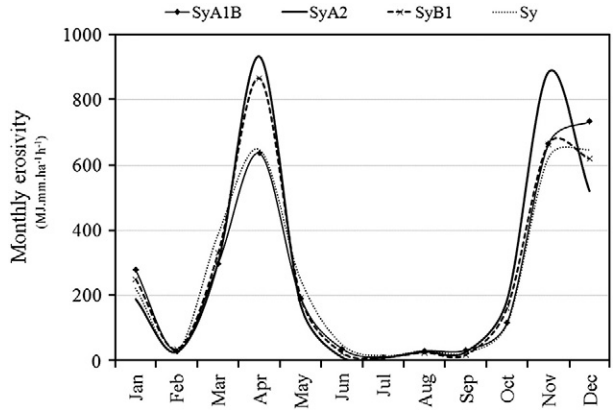

Fig. 6. Monthly distribution of the rainfall erosivity obtained using the synthetic precipitation datasets.

The average *R* factor for the study area was approximately 3040 MJ mm ha^{-1} h^{-1} $year^{-1}$ for the Sy scenario, which simulates the observed historical precipitation variability. This result is consistent with figures obtained in other semi-arid regions. For instance, Da Silva (2004) found that erosivity varied from 2000 to 4000 MJ mm ha^{-1} h^{-1} $year^{-1}$ in semi-arid regions in north-eastern Brazil. However, the present results show that in regions with high topographic heterogeneity, such as the Taita Hills, it is crucial to consider local variations at detailed spatial scales. In this case, the *R* factor in the study area varied from 160 MJ mm ha^{-1} h^{-1} $year^{-1}$ in lowlands to approximately 6000 MJ mm ha^{-1} h^{-1} $year^{-1}$ in the highlands. The global average also masks important variations brought by potential climate changes. For instance, while the absolute difference between the *R* factor averages for the Sy and SyA2 scenarios was around 250 MJ mm ha^{-1} h^{-1} $year^{-1}$, local changes reached 1500 MJ mm ha^{-1} h^{-1} $year^{-1}$ in some regions in the highlands.

Additionally to the importance of spatial variability at local scales, understanding seasonal variations was shown to be essential to delineate appropriate strategies and cope with climate changes. The importance of seasonal analysis on rainfall erosivity has already been demonstrated in previous studies. For instance, to evaluate changes in rainfall erosivity in southern Italy, Diodato and Bellocchi (2009) demonstrated that soil erosion risk tends to rise predominantly between April and November, as a consequence of increasing climate erosive hazard. Munka et al. (2007) studied the variation in rainfall erosivity in Uruguay between 1931 and 2000, evidencing that spatial aspects of erosivity changes are closely dependent on seasonal variations.

In the present study, the most critical rainfall erosivities occurred during April and November. It is interesting to note that the most aggressive climate change scenario during these months (SyA2)

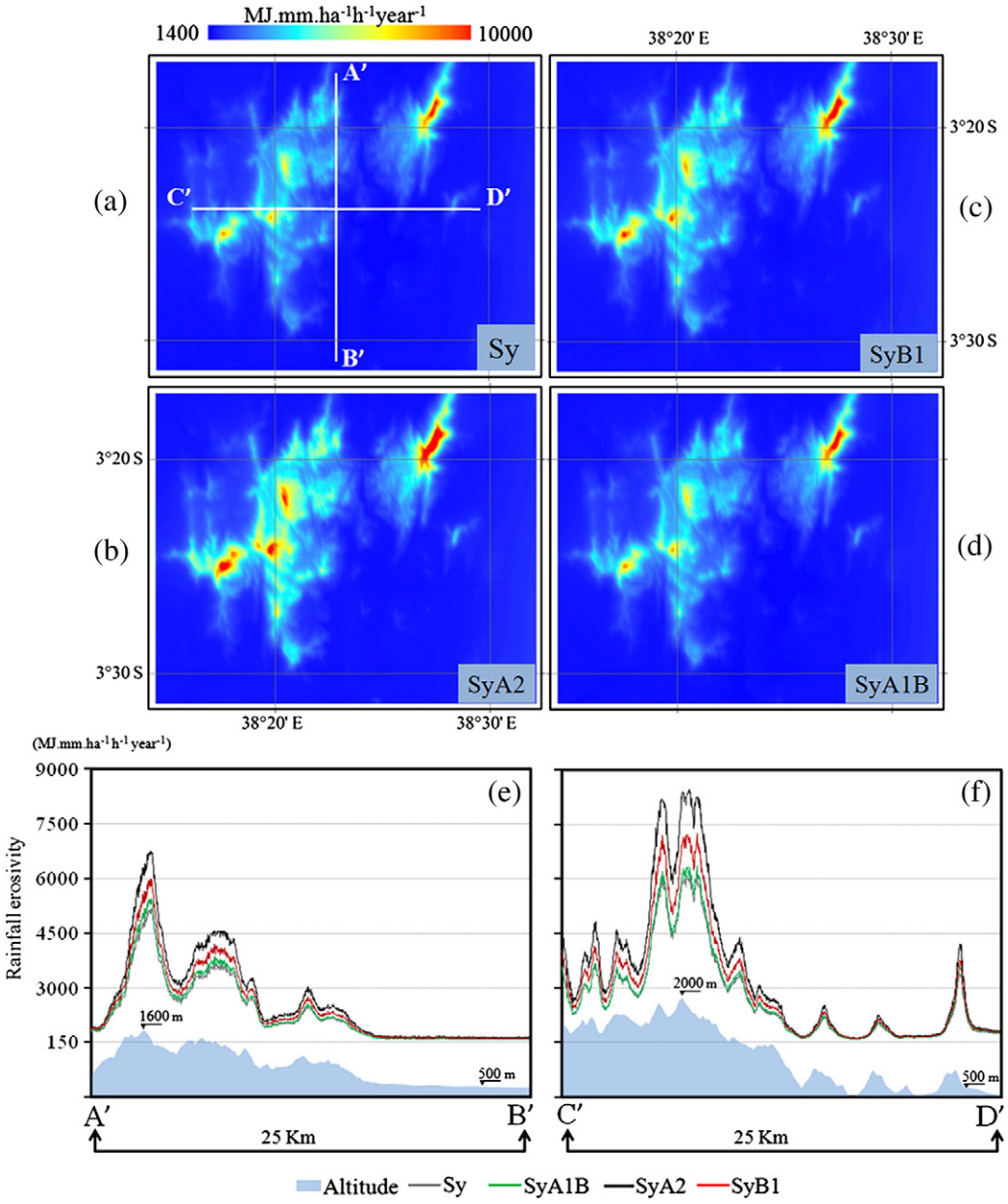

Fig. 7. Maps showing the spatial distribution of the USLE *R* factor in the study area. (a) Sy scenario; (b) SyA2 scenario; (c) SyB1 scenario; (d) SyA1B scenario; (e) spatial profile of the *R* factor along the transect A′–B′ and (f) spatial profile of the *R* factor along the transect C′–D′.

retrieved the highest decreases in erosivity during December and January. On the other hand, the most conservative SyA1B scenario resulted in the lowest annual average increase (0.7%) and retrieved the highest increases also during December and January (25% and 13%, respectively).

From the practical point of view, it is important to analyse these changes together with other attributes that are directly associated with the soil susceptibility to rainfall erosivity. For instance, the vegetation cover in agricultural areas, which can protect the soil against the impact of rainfall, varies significantly during the year. In general the seeding and harvest seasons are the most critical, since during these periods the soil is not protected by any vegetation cover. According to Kenya's Ministry of Agriculture, the periods from February to March and from June to October are typical for harvesting and seeding in the Taita Hills (Fig. 9b,c). This information is confirmed by the Normalized Difference Vegetation Index (*NDVI*) temporal profile extracted from 50 random points in the agricultural areas from 2001 to 2008 using satellite images from the MODIS/Terra sensor (Fig. 9a; Maeda, 2009). *NDVI* is closely related to crops' phenology and biomass production.

Evidently, the agricultural calendar is adjusted according to historical rainfall pattern. Hence, the months with higher rainfall usually coincide with periods of maximum vegetation vigour, and the months of lower rainfall with the seeding and harvest seasons. In the present study, no significant increases in rainfall erosivity were observed in the climate change scenarios during the months when harvest and seeding take place. The main concern from this point of view is the decreases in rainfall volume observed in March and May, which will extend the dry seasons in the Taita Hills and potentially affect the agricultural calendar. This fact may obligate producers to move the seeding season to months with higher precipitation and, consequently, higher erosivity.

Changes in erosion control practices (*P* factor) were not considered in the present study. However, previous studies have shown that appropriate land management can significantly decrease soil erosion.

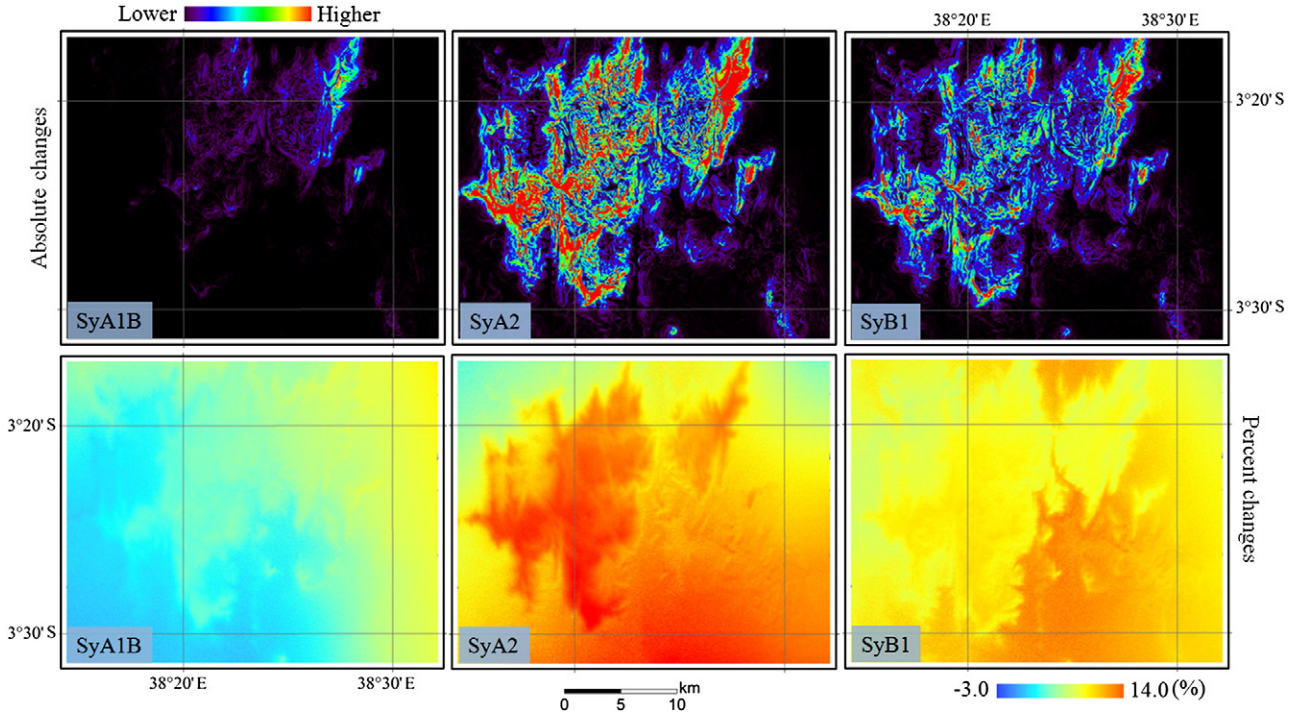

Fig. 8. Absolute and percent changes in the soil erosion potential.

For instance, studying soil erosion risk scenarios in Calabria, southern Italy, Terranova et al. (2009) showed that erosion control practices can cause a significant reduction of the erosion rate from roughly 30 to 12.3 Mg ha^{-1} $year^{-1}$. Feng et al. (2010) demonstrated that soil conservation measures taken by the Chinese government (Grain-for-Green project) significantly decreased soil erosion in the Loess Plateau between the years 1990 and 2005. Hence, further analysis must be carried out to evaluate the potential of using alternative erosion control practices in the Taita Hills aiming at the mitigation of erosivity increases caused by climate change.

Although it was not possible to assess the influence of the soil map spatial resolution for this specific study case, the KENSOTER datasets have been successfully applied in previous studies in Kenya. Namely, these data have recently been used for the assessment of soil carbon stocks and change in Kenya (Milne et al., 2007). Furthermore, Levick et al. (2004) evaluated the impacts of different soil maps' spatial scales on the outputs of a hydrologic modelling tool. By comparing maps with scales of 1:15,000, 1:250,000 and 1:5,000,000, the authors concluded that results obtained with the coarser scale soil map were adequate for estimating surface runoff, producing results comparable to the map with the higher resolution. Nevertheless, it is perhaps obvious that, in considering the specific case of soil erosion studies, the effects of different soil map scales may be more noticeable.

The spatial resolution (20 m) and vertical accuracy (± 8 m) of the DEM used in this study are consistent with previous studies and considered adequate for this kind of assessments. According to Rojas et al. (2008), in general, very good modelling results are obtained at grid sizes between 30 and 90 m. Nevertheless, Verstraeten (2006) warns that coarser resolution DEMs may reduce the average erosion rate by smoothing steep topography and, in these cases, the calibration coefficients of models need to be adjusted in order to compensate for the differences.

Concerning the uncertainties involved in the modelling framework applied in this research, two main sources can be highlighted. Firstly, the agricultural expansion rates used to simulate the LUCC scenarios did not take into account changes in socio-economic aspects, which may increase or decrease the expansion rates. However, although LUCC rates may vary over time, it is still reasonable to expect that the calibrated model is effective in indicating the areas with a higher probability of change. The other main source of uncertainty concerns the error accumulation in the construction of the synthetic precipitation datasets. Besides the uncertainties intrinsic to the scenarios simulated by the GCM, which includes uncertainties on chemical, physical, and socio-economic aspects (Kerr, 2001), the simplified approach used in this study to represent the climate variations at a higher spatial scale incorporates additional uncertainties into the scenarios. Nevertheless, it is worth emphasizing that the importance of this kind of study is not to give a precise picture of the future but to provide scientists and policy makers with a comprehensive understanding of the possible future scenarios.

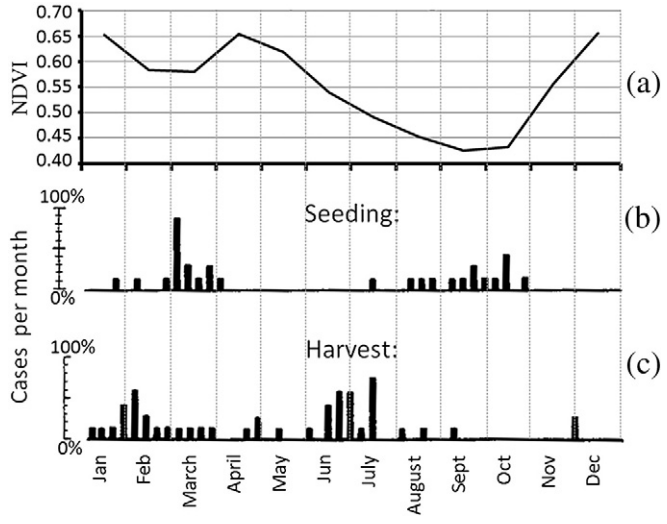

Fig. 9. Phenology in croplands and agricultural calendar in the study area. (a) *NDVI* temporal profile from cropland areas obtained using satellite images from the MODIS/Terra sensor from 2001 to 2008 (after Maeda, 2009). (b) Maize seeding calendar in the Taita Hills. (c) Maize harvest calendar in the Taita Hills.
After Jaetzold and Schmidt, 1983.

6. Conclusions

Changes in precipitation patterns inevitably affect soil erosion by changing the amount of energy available in rainfall to detach and carry sediments. It is also clear, based on numerous scientific studies, that LUCC caused by agricultural expansion can accelerate soil loss. The establishment of feasible and fast strategies to cope with such changes is an essential step in the direction of soil conservation. This study has demonstrated that by understanding the interactions of climatic variations, LUCC and landscape attributes, it is possible to evaluate the impacts of environmental changes and indicate priority regions from the soil conservation point of view.

The results of the LUCC simulation indicate that agricultural expansion in the Taita Hills is driving into areas with less pronounced slopes, lower precipitation and, consequently, lower soil erosion potential. Nevertheless, if current trends persist, it is expected that agricultural areas will occupy 60% of the study area by 2030. These changes will increase the USLE *C* factor in up to 8.8%, resulting in accelerated soil erosion.

A large contrast was observed among the different climate scenarios described in the synthetic precipitation datasets generated for this study. Despite this fact, important tendencies can be clearly identified. By the year 2030, rainfall erosivity is likely to increase during April and November. All scenarios converge to a slight erosivity decrease tendency during March and May. The highest uncertainties were observed in January and December, when some scenarios indicate a small reduction in erosivity while some indicate an increase.

Accounting for LUCC and climate changes in an integrated manner, we can conclude that the highlands of the Taita Hills must be prioritized for soil conservation policies during the next 20 years. Although new croplands are likely to be settled in lowlands over the next decades, increases in precipitation volumes are expected to be higher in the highlands. Moreover, it was demonstrated that in areas with elevated *LS* factor values, typically in the highlands, increases in rainfall will have significantly higher impacts on soil erosion potential.

Acknowledgements

This study was funded by the Academy of Finland, the Centre for International Mobility (CIMO) and the University of Helsinki Research Foundation.

References

Alcamo, J., 2001. Scenarios as Tools for International Environmental Assessments, Experts Corner Reports — Prospects and Scenarios No. 5. European Environment Agency, Copenhagen.

Almeida, C.M., Vieira Monteiro, A.M., Camara, G., Soares-Filho, B.S., Coutinho, Cerqueira G., Lopes, Pennachin C., Batty, M., 2005. GIS and remote sensing as tools for the simulation of urban land-use change. International Journal of Remote Sensing 26, 759–774.

Bakker, M.M., Govers, G., Jones, R.A., Rounsevell, M.D.A., 2007. The effect of soil erosion on Europe's crop yields. Ecosystems 10, 1209–1219.

Batjes, N.H., Gicheru, P., 2004. Soil Data Derived from SOTER for Studies of Carbon Stocks and Change in Kenya (ver. 1.0; GEFSOC Project). Report 2004/01. ISRIC — World Soil Information, Wageningen.

Batjes, N.H., Al-Adamat, R., Bhattacharyya, T., Bernoux, M., Cerri, C.E.P., Gicheru, P., Kamoni, P., Milne, E., Pal, D.K., Rawajfih, Z., 2007. Preparation of consistent soil data sets for modelling purposes: secondary SOTER data for four case study areas. In: Milne, E., Powlson, D.S., Cerri, C.E.P. (Eds.), Soil Carbon Stocks at Regional Scales: Agriculture, Ecosystems & Environment, 122, pp. 26–34.

Beskow, S., Mello, C.R., Norton, L.D., Curi, N., Viola, M.R., Avanzi, J.C., 2009. Soil erosion prediction in the Grande River Basin, Brazil using distributed modelling. Catena 79, 49–59.

Brink, A.B., Eva, H.D., 2009. Monitoring 25 years of land cover change dynamics in Africa: a sample based remote sensing approach. Applied Geography 29, 501–512.

Burgess, N.D., Butynski, T.M., Cordeiro, N.J., Doggart, N.H., Fjeldsa, J., Howell, K.M., Kilahama, F.B., Loader, S.P., Lovett, J.C., Mbilinyi, B., Menegon, M., Moyer, D.C., Nashanda, E., Perkin, A., Rovero, F., Stanley, W.T., Stuart, S.N., 2007. The biological importance of the Eastern Arc Mountains of Tanzania and Kenya. Biological Conservation 134, 209–231.

Clark, B., 2010. Enhanced Processing of SPOT Multispectral Satellite Imagery for Environmental Monitoring and Modelling. University of Helsinki, Faculty of Science, Doctoral dissertation978-952-10-6306-0.

Clark, B.J.F., Pellikka, P.K.E., 2009. Landscape analysis using multiscale segmentation and object orientated classification. In: Röder, A., Hill, J. (Eds.), Recent Advances in Remote Sensing and Geoinformation Processing for Land Degradation Assessment. ISPRS Book Series in Photogrammetry, Remote Sensing and Spatial Information Sciences, Vol. 8. Taylor & Francis, London, pp. 323–342.

Da Silva, A.M., 2004. Rainfall erosivity map for Brazil. Catena 57, 251–259.

Diodato, N., Bellocchi, G., 2009. Assessing and modelling changes in rainfall erosivity at different climate scales. Earth Surface Processes and Landforms 34, 969–980.

Erdogan, E.H., Pellikka, P., Clark, B., in press. Impact of land cover change on soil loss in the Taita Hills, Kenya between 1987 and 2003. International Journal of Remote Sensing.

Feng, X., Wang, Y., Chen, L., Fu, B., Bai, G., 2010. Modeling soil erosion and its response to land-use change in hilly catchments of the Chinese Loess Plateau. Geomorphology 118, 239–248.

Fischer, G., Tubiello, F.N., van Velthuizen, H., Wiberg, D.A., 2007. Climate change impacts on irrigation water requirements: effects of mitigation, 1990 2080. Technological Forecasting and Social Change 74, 1083–1107.

Foley, J., de Fries, R., Defries, R., Asner, G.P., Barford, C., Bonan, G., Carpenter, S.R., Chapin, F.S., Coe, M.T., Daily, G.C., Gibbs, H.K., Helkowski, J.H., Holloway, T., Howard, E., Kucharik, C.J., Monfreda, C., Patz, J., Prentice, I.C., Ramankutty, N., Snyder, P.K., 2005. Global consequences of land use. Science 309, 570–574.

Fournier, H., 1960. Climat et erosion. Ed. Presses Universitaires de France, Paris.

García-Ruiz, J.M., 2010. The effects of land uses on soil erosion in Spain: a review. Catena 81, 1–11.

Hagen, A., 2003. Fuzzy set approach to assessing similarity of categorical maps. International Journal of Geographical Information Science 17, 235–249.

Husak, G.J., Michaelsen, J., Funk, C., 2007. Use of the gamma distribution to represent monthly rainfall in Africa for drought monitoring applications. International Journal of Climatology 27, 935–944.

Hutchinson, M.F., 1995. Interpolating mean rainfall using thin plate smoothing splines. International Journal of Geographical Information Science 9, 305–403.

IPCC (Intergovernmental Panel on Climate Change), 2007. Summary for Policymakers: Synthesis Report. Paris.

Istvánovics, V., 2009. Eutrophication of lakes and reservoirs. In: Likens, G.E. (Ed.), Encyclopedia of Inland Waters. Academic Press, London, pp. 157–165. doi:10.1016/B978-012370626-3.00141-1.

Jaetzold, R., Schmidt, H., 1983. Farm Management Handbook of Kenya, vol. II. East Kenya. Ministry of Agriculture, Kenya.

Kepner, W.G., Semmens, D.J., Bassett, S.D., Mouat, D.A., Goodrich, D.C., 2004. Scenario analysis for the San Pedro River, analysing hydrological consequences of a future environment. Environmental Monitoring and Assessment 94, 115–127.

Kerr, R.A., 2001. Global warming: rising global temperature, rising uncertainty. Science 292 (5515), 192–194.

Kinnell, P.I.A., 2010. Event soil loss, runoff and the Universal Soil Loss Equation family of models: a review. Journal of Hydrology 385, 384–397.

Kirkby, M.J., Bracken, L.J., 2009. Gully processes and gully dynamics. Earth Surface Processes and Landforms 34, 1841–1851.

Koomen, E., Rietveld, P., Nijs, T.de., 2008. Modelling land-use change for spatial planning support. The Annals of Regional Science 42, 1–10.

Levick, L.R., Semmens, D., Guertin, D.P., Burns, I.S., Scott, S.N., Unkrich, C.L., Goodrich, D.C., 2004. Adding Global Soils Data to the Automated Geospatial Watershed Assessment Tool (AGWA). Proceedings 2nd SAHRA, (Sustainability of Semi-Arid Hydrologic and Riparian Areas). University of Arizona, International Symposium on Transboundary Water Management, Tucson, pp. 1–9.

Maeda, E.E., 2009. Impacts of Agricultural Expansion on Irrigation Water Requirements in Taita Hills, Kenya. Interim Report IR-09-056. International Institute for Applied Systems Analysis, Laxenburg, Austria.

Maeda, E.E., Formaggio, A.R., Shimabukuro, Y.E., 2008. Impacts of land use and land cover changes on sediment yield in a Brazilian Amazon drainage basin. GIScience & Remote Sensing 45, 443–453.

Maeda, E.E., Clark, B.J.F., Pellikka, P.K.E., Siljander, M., 2010. Modelling agricultural expansion in Kenya's Eastern Arc Mountains biodiversity hotspot. Agricultural Systems. doi:10.1016/j.agsy.2010.07.004.

McHugh, M.J., 2005. Multi-model trends in East African rainfall associated with increased CO_2. Geophysical Research Letters 32, L01707. doi:10.1029/2004GL021632.

Merritt, W.S., Letcher, R.A., Jakeman, A.J., 2003. A review of erosion and sediment transport models. Environmental Modelling and Software 18, 761–799.

Miller, S.N., Kepner, W.G., Mehaffey, M.H., Hernandez, H., Miller, R.C., Goodrich, D.C., Devonald, K.K., Heggem, D.T., Miller, W.P., 2002. Integrating landscape assessment and hydrologic modeling for land cover change analysis. Journal of the American Water Resources Association 38, 915–929.

Milne, E., Al Adamat, R., Batjes, N.H., Bernoux, M., Bhattacharyya, T., Cerri, C.C., Cerri, C.E.P., Coleman, K., Easter, M., Falloon, P., Feller, C., Gicheru, P., Kamoni, P., Killian, K., Pal, D.K., Paustian, K., Powlson, D.S., Rawajfih, Z., Sessay, M., Williams, S., Wokabi, S., 2007. National and sub-national assessments of soil organic carbon stocks and changes: the GEFSOC modelling system. Agriculture, Ecosystems & Environment 122, 3–12.

Munka, C., Cruz, G., Caffera, R.M., 2007. Long term variation in rainfall erosivity in Uruguay: a preliminary Fournier approach. GeoJournal 70, 257–262.

Nakicenovic, N., Alcamo, J., Davis, G., de Vries, B., Fenhann, J., Gaffin, S., Gregory, K., Grübler, A., Jung, T.Y., Kram, T., Lebre la Rovere, E., Michaelis, L., Mori, S., Morita, T., Pepper, W., Pitcher, H., Price, L., Riahi, K., Roehrl, A., Rogner, H.H., Sankovski, A., Schlesinger, M., Shukla, P., Smith, S., Swart, R., van Rooijen, S., Victor, N., Dadi, Z., 2000. Emissions Scenarios: A Special Report of the Intergovernmental Panel on Climate Change (IPCC). Cambridge University Press, Cambridge. 509p.

Nigel, R., Rughooputh, S., 2010. Mapping of monthly soil erosion risk of mainland Mauritius and its aggregation with delineated basins. Geomorphology 114, 101–114.
Pellikka, P.K.E., Lötjönen, M., Siljander, M., Lens, L., 2009. Airborne remote sensing of spatiotemporal change (1955 2004) in indigenous and exotic forest cover in the Taita Hills, Kenya. International Journal of Applied Earth Observations and Geoinformation 11, 221–232.
Rahman, M.R., Shi, Z.H., Chongfa, C., 2009. Soil erosion hazard evaluation — an integrated use of remote sensing, GIS and statistical approaches with biophysical parameters towards management strategies. Ecological Modelling 220, 1724–1734.
Renard, K.G., Freimund, J.R., 1994. Using monthly precipitation data to estimate the R factor in the revised USLE. Journal of Hydrology 157, 287–306.
Renard, K.G., Foster, G.R., Weesies, G.A., McCool, D.K., Yoder, D.C., 1997. Predicting Soil Erosion by Water: A Guide to Conservation Planning with the Revised Universal Soil Loss Equation (RUSLE). USDA Agric Handbook 703. 384pp.
Republic of Kenya, 2001. The 1999 Population & Housing Census. Central Bureau of Statistics, Ministry of Planning and National Development, Kenya.
Rojas, R., Velleux, M., Julien, P.Y., Johnson, B.E., 2008. Grid scale effects on watershed soil erosion models. Journal of Hydrologic Engineering 13, 793–802.
Schiettecatte, W., D'hondt, L., Cornelis, W.M., Acosta, M.L., Leal, Z., Lauwers, N., Almoza, Y., Alonso, G.R., Díaz, J., Ruíz, M., Gabriels, D., 2008. Influence of landuse on soil erosion risk in the Cuyaguateje watershed (Cuba). Catena 74, 1–12.
Schmidhuber, J., Tubiello, F.N., 2007. Global food security under climate change. Proceedings of the National Academy of Sciences 104, 19703–19708.
Sirviö, T., Rebeiro-Hargrave, A., Pellikka, P., 2004. Geoinformation in Gully Erosion Studies in the Taita Hills, SE-Kenya, Preliminary Results. Proceedings of the 5th AARSE conference (African Association of Remote Sensing of the Environment), 18–21 October, 2004. CD-Publication, Nairobi, Kenya.
Soares-Filho, B.S., Pennachin, C.L., Cerqueira, G., 2002. DINAMICA — a stochastic cellular automata model designed to simulate the landscape dynamics in an Amazonian colonization frontier. Ecological Modelling 154, 217–235.
Soares-Filho, B.S., Rodrigues, H., Costa, W., 2009. Modeling Environmental Dynamics with Dinamica EGO1st Ed. Belo Horizonte. 115p.
Terranova, O., Antronico, L., Coscarelli, R., Iaquinta, P., 2009. Soil erosion risk scenarios in the Mediterranean environment using RUSLE and GIS: an application model for Calabria (southern Italy). Geomorphology 112, 228–245.
Thornton, P.K., Jones, P.G., Alagarswamy, G., Andresen, J., 2009. Spatial variation of crop yield response to climate change in East Africa. Global Environmental Change 19, 54–65.
Thornton, P.K., Jones, P.G., Alagarswamy, G., Andresen, J., Herrero, M., 2010. Adapting to climate change: agricultural system and household impacts in East Africa. Agricultural Systems 103, 73–82.
Valentin, C., Poesen, J., Li, Y., 2005. Gully erosion: impacts, factors and control. Catena 63, 132–153.
Van Oost, K., Govers, G., Desmet, P., 2000. Evaluating the effects of changes in landscape structure on soil erosion by water and tillage. Landscape Ecology 15, 577–589.
Veldkamp, T., Lambin, E.F., 2001. Predicting land-use change. Editorial. Special issue. Agriculture, Ecosystems & Environment 85, 1–6.
Verstraeten, G., 2006. Regional scale modelling of hillslope sediment delivery with SRTM elevation data. Geomorphology 81, 128–140.
Wilks, D., 1990. Maximum likelihood estimation for the gamma distribution using data containing zeros. Journal of Climate 3, 1495–1501.
Williams, J.R., Renard, K.G., 1983. EPIC: a new method for assessing erosion's effects on soil productivity. Journal of Soil and Water Conservation 38, 381–383.
Wischmeier, W.H., Smith, D.D., 1978. Predicting Rainfall Erosion Losses. A Guide to Conservation Planning. United States Department of Agriculture, Agricultural Handbook #537, p. 58.
Xiaodan, W., Xianghao, Z., Jianrong, F., 2004. Assessment and spatial distribution of sensitivity of soil erosion in Tibet. Journal of Geographical Sciences 14, 41–46.
Yang, D., Kanae, S., Oki, T., Koike, T., Musiake, K., 2003. Global potential soil erosion with reference to land use and climate changes. Hydrological Processes 17, 2913–2928.
Zuazo, V.H.D., Pleguezuelo, C.R.R., 2008. Soil-erosion and runoff prevention by plant covers. A review. Agronomy for Sustainable Development 28, 65–86.